ORNL-4698
Special

DIFFERENTIAL CROSS SECTIONS AT FORWARD ANGLES FOR HYDROGEN AND HELIUM PARTICLES FROM 62-MeV PROTONS INCIDENT ON ^{60}Ni

R. W. Peelle
F. E. Bertrand

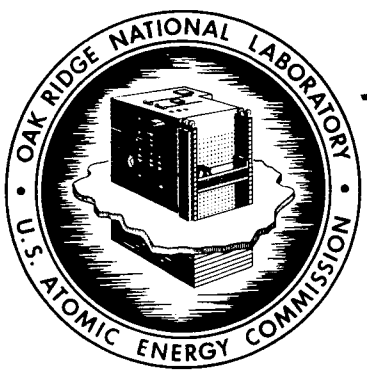

OAK RIDGE NATIONAL LABORATORY
operated by
UNION CARBIDE CORPORATION
for the
U.S. ATOMIC ENERGY COMMISSION

ORNL-4698

Contract No. W-7405-eng-26

Neutron Physics Division

DIFFERENTIAL CROSS SECTIONS AT FORWARD ANGLES FOR HYDROGEN AND HELIUM PARTICLES FROM 62-MeV PROTONS INCIDENT ON ^{60}Ni

R. W. Peelle and F. E. Bertrand

NOTE

This Work Funded by
NATIONAL AERONAUTICS AND SPACE ADMINISTRATION
Under Order L-12, 186

JUNE 1971

OAK RIDGE NATIONAL LABORATORY
Oak Ridge, Tennessee
operated by
UNION CARBIDE CORPORATION
for the
U. S. ATOMIC ENERGY COMMISSION

DIFFERENTIAL CROSS SECTIONS AT FORWARD ANGLES FOR HYDROGEN AND HELIUM PARTICLES FROM 62-MeV PROTONS INCIDENT ON ^{60}Ni

R. W. Peelle and F. E. Bertrand

Abstract

Tabulated differential cross sections are presented for the production, at angles of 15, 20, 25, and 40 deg, of proton, deuteron, triton, helium-3, and alpha particles from ^{60}Ni bombarded by 62-MeV protons. Continuum cross sections are listed in ~ 1-MeV bins for energies above lower cutoffs which range from 4 to 15 MeV for the different types of exit particles. For a considerable energy range within each spectrum, only the integral cross section is known. The proton-, deuteron-, and alpha-particle cross sections are the same in the continuum region above the evaporation peak as those cross sections previously observed for ^{54}Fe and ^{56}Fe, but the corresponding yield of tritons is higher from ^{60}Ni and ^{56}Fe than from ^{54}Fe.

INTRODUCTION

Differential cross sections are tabulated in this report for proton, deuteron, triton, helium-3, and alpha particles produced in the range 15 to 40 deg in a target of ^{60}Ni under bombardment by 61.7-MeV protons. The lower limit on the energy of the outgoing particle was determined by the energy of a particle just stopped in the first ΔE detector (~ 100-μ silicon). A flaw in the experimental setup, involving an errant piece of drafting tape between adjacent detectors, makes the data here less precise than that presented elsewhere for neighboring elements in that each spectrum includes a region for which only the average magnitude is known. The details of the experimental and data analysis system have been reported,[1-3] and the results for ^{54}Fe and ^{56}Fe used for comparison have been tabulated elsewhere.[4] The tabulated

values for other targets from this experiment may be found in reports cited in ref. 5.

METHOD AND DATA ANALYSIS

Momentum-analyzed protons from the Oak Ridge Isochronous Cyclotron were focussed to an ~8-mm spot on a target of ^{60}Ni. The charged reaction products were detected by a semiconductor telescope spectrometer with ~180 keV resolution mounted within a 1.2-m-diam evacuated scattering chamber. The telescope consisted of two silicon surface-barrier ΔE detectors, 100 and 500 μ in thickness, and a planar Ge(Li) stopping detector.[6] For each event, data were obtained from three analog-to-digital converters and written onto compatible magnetic tape by an on-line PDP-8 computer for later analysis on the Laboratory's central computer. Secondary particles were identified by a twofold $\Delta E \times E$ method over the energy range from a few MeV (set by penetration of the 100-μ detector) to 62 MeV. The ^{54}Fe data shown in the figures has a lower energy cutoff since time-of-flight particle identification was used for those particles which stopped in the 100-μ detector.

Table 1 gives a list of the factors by which counts in the various runs were multiplied to give laboratory-system cross sections in millibarns/steradian. These factors are based on the foil thickness and geometry, the detector solid angle, and the electric charge collected by a carefully constructed Faraday cup. (See ref. 1, pages 46 and 81.)

The >99% isotopically pure ^{60}Ni target was fabricated by the Isotopes Division of the Oak Ridge National Laboratory. The average surface density was 3.8 mg/cm;[2] a 4% uncertainty was assigned because a detailed scan for uniformity could not be performed.

Table 1. Conversion Factors for the ^{60}Ni Experimental Runs.

Laboratory Angle (deg)	Run Number	Factor ($mb \cdot ster^{-1} \cdot count^{-1}$)
15	5003	4.74 (-3)[a]
20	5004	2.53 (-3)
25	5005	1.295 (-3)
40	5006	7.89 (-4)

[a]Read as 4.74×10^{-3}

The data tabulated in this report have been corrected to remove in first order the effects of energy loss of scattered particles in the target, penetration of the edges of the detector collimator, multiple scattering of secondary protons by the ΔE detectors, the "dead" layer covering the germanium detector, and nuclear reactions of hydrogen particles in the Ge detector. The correction techniques are described in refs. 1 and 2. The dead layer over the Ge detector was normally about 3 mg/cm^2 of nickel, but for the data presented here a protective layer of masking tape was inadvertently left in the same region between the ΔE detectors and the stopping detector. On-line diagnostic graphics clearly showed the effect of this layer; there was insufficient time to repeat the runs which led to the data presented here. Moreover, the surface density of the tape was not measured when the mistake was discovered, since at that time there was no intention to study the continuum data from this target. The appropriate dead layer for the analysis was determined by weighing a "typical" piece of masking tape, and also by performing our standard dead layer correction with a few different thicknesses of plastic (Mylar) to represent the masking tape and requiring internal consistency among the diagnostic outputs available. The layer was finally taken as 15 mg/cm^2 mylar, with an uncertainty of < 5 mg/cm^2.

The effect of the dead layer is to 1) leave empty a portion of the spectrum corresponding to the energy region in which particles stop in the dead layer, 2) to place spurious "fold back" counts at lower energies corresponding to the energy actually lost in the ΔE counters, and 3) to

displace events which did count in the stopping detector to an incorrectly low value. Counts are conserved within the affected region, so for the data presented here this entire region is represented by one broad histogram block. The third difficulty is corrected in first order by the standard correction program. The largest uncertainty from this effect is in the cross sections presented for the energies just above the broad blocks, and is about 7% based on a 5 mg/cm^2 uncertainty in the thickness of the dead layer. A fourth difficulty was that some alpha-particle events were shifted by the dead-layer correction to an impossibly high energy, indicating an overcorrection. The results in this region are presented as a broad histogram block.

Data tables and graphs below show statistical uncertainties propagated from the Poisson uncertainties in the experimental counts. To obtain the full uncertainty on a given cross section, the statistical uncertainties must be combined with an overall systematic uncertainty and a few special systematic uncertainties, described below, which affect limited regions of the spectra. The overall systematic uncertainty is estimated to be $\sim \pm 7\%$ for these data, including uncertainties in foil weight, detector solid angle, number of incident protons, and dead time fraction.

Systematic uncertainty is increased to $\sim 10\%$ for areas of low cross section, such as most of the ^3He data, because the lines in $\Delta E \times E$ space which distinguish events among the particle types are derived empirically on the basis of observed events. Scattered counts are not always detected in the diagnostic computer outputs which exhibit the fit between the data and the imposed "discrimination lines."

The magnitudes of the "tail" correction for nuclear reactions in the Ge(Li) detector and for collimator edge penetration are both dependent upon the number and spectral distribution of the recorded counts. The reaction correction has two components; 1) a correction at each channel to add back the counts lost and 2) a correction to remove at each channel the counts added by reactions of higher energy events. Both of these effects have been corrected. The latter reaction correction and the collimator edge correction are significantly large only for protons at scattering angles < 30 deg, where the spectra are dominated by strong elastic scattering, and the corrections generally fall rapidly with angle within that range. The uncertainty in the correction for collimator penetration is taken as 20% of the correction, which is approximately proportional to pulse height. This uncertainty is significant only for the data at 15 deg, as shown in Table 2. The reaction-tail correction (type 2) rises from zero to its full value between 35 and 45 MeV and then remains roughly constant up to the elastic peak. The cross section uncertainty in the standard reaction-tail correction, taken as 25% of that correction, is given in Table 2.

RESULTS

No results are given here for excitation of specific levels of the residual nuclei, since too few angles are included to allow generally meaningful results. Some results from this work have been published for excitation of the 1.33-MeV level of ^{60}Ni (ref. 7).

To illustrate the results for ^{60}Ni, comparisons are shown with data for ^{54}Fe and ^{56}Fe (ref. 4). Figures 1 and 2 show comparisons between targets of ^{54}Fe and ^{60}Ni for secondary protons and for alpha particles,

Table 2. Systematic Uncertainties in Secondary Proton Cross Sections at 45 MeV from Reaction-Tail and Collimator-Tail Corrections.

Laboratory Angle	Uncertainties in Corrections Applied	
	"Collimator Tail"	"Reaction Tail"
	$mb \cdot ster^{-1} \cdot MeV^{-1}$	$mb \cdot ster^{-1} \cdot MeV^{-1}$
15	0.14	0.52
20	0.026	0.10
25	0.007	0.02
40	0.004	0.01

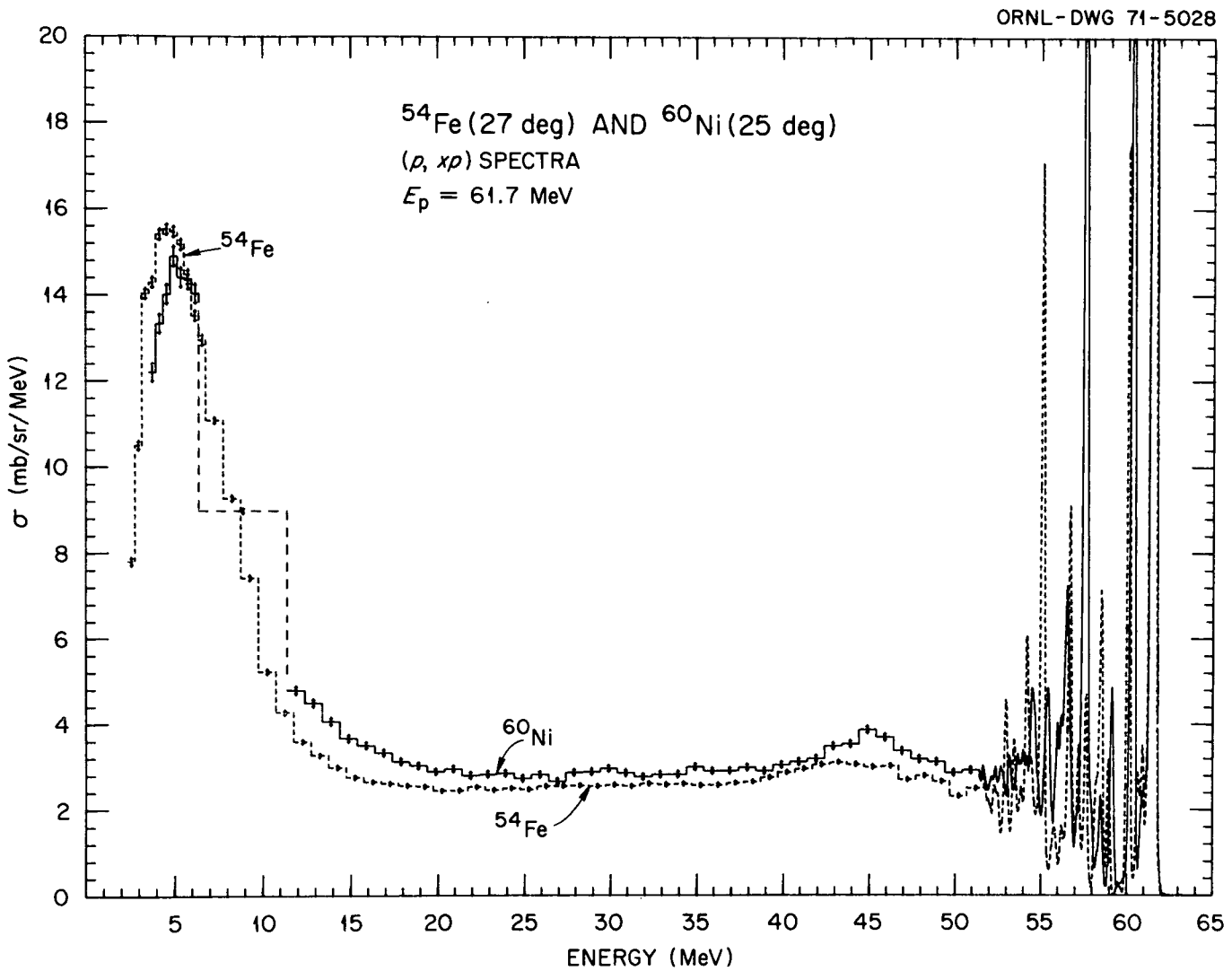

Fig. 1. Proton Spectra from 62-MeV Protons on ^{60}Ni at 25 deg and ^{54}Fe at 27 deg. The broad dashed bin near 10 MeV in the otherwise-solid line represents the average cross section for ^{60}Ni(p,xp) in the region where cross sections were affected by the unusually thick dead layer.

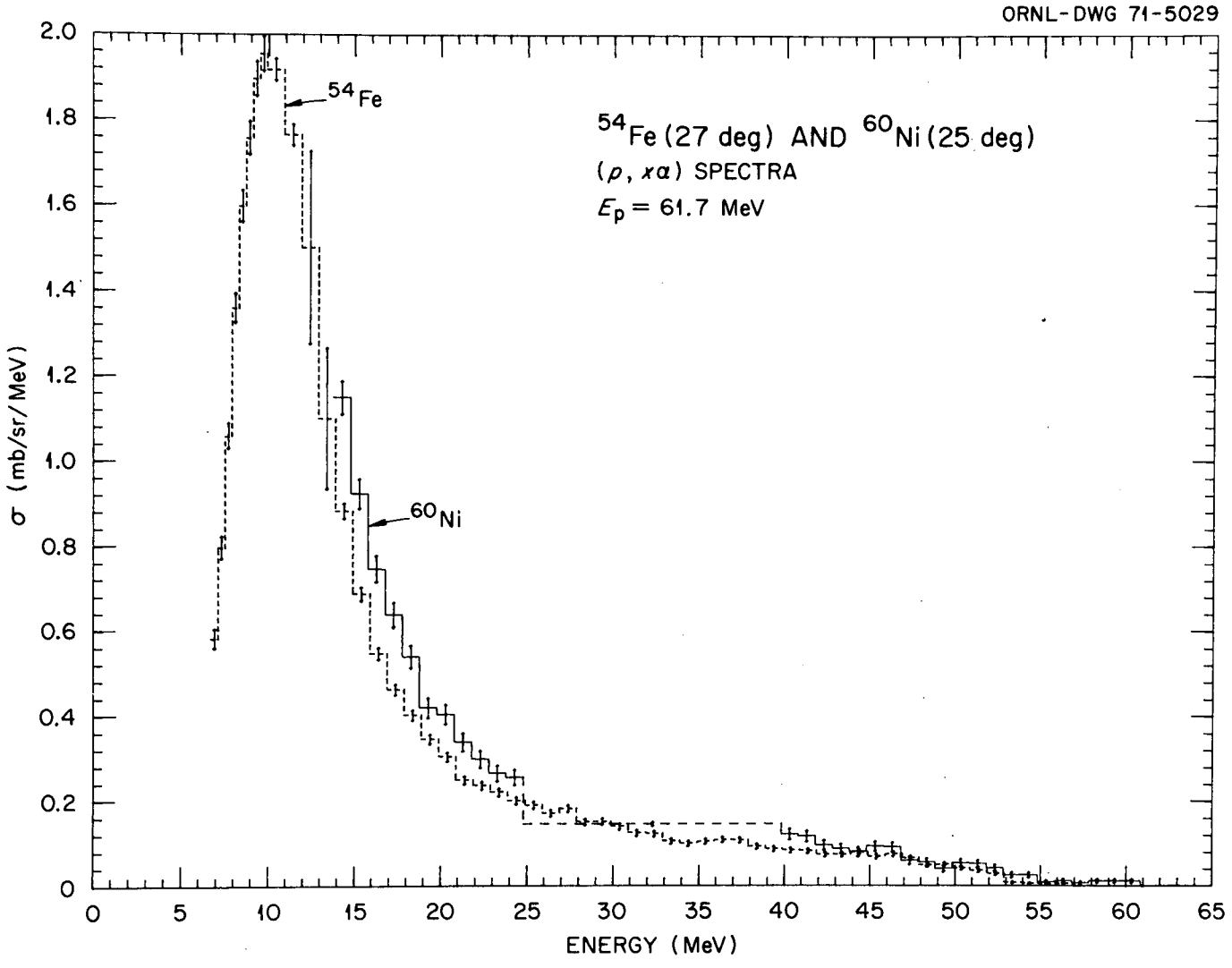

Fig. 2. Alpha-particle Spectra from 62-MeV Protons on ^{60}Ni at 25 deg and ^{54}Fe at 27 deg. The broad dashed bin near 30 MeV in the otherwise-solid line represents the average cross section for ^{60}Ni(p,xα) in the region where cross sections were affected by the dead layer.

but for angles smaller than 25 deg proton comparisons are ambiguous. Figure 3 shows data for all three targets for protons at ~40 deg. Note that the ^{56}Fe data is really at 37 deg and that a gap in existing data appears for ^{54}Fe in the region between 6 and 15 MeV. For the cases in Figs. 1-3, it appears that cross sections above the evaporation region are strictly comparable, while in the evaporation region other factors determine the cross section. For example, one would expect relatively more proton than neutron evaporation for the proton rich ^{54}Fe, as shown in Fig. 3.

Figure 4 shows the comparison of deuteron spectra observed at 20 deg for the three targets. The results at 15 deg are similar. The importance of the level structure leads to a confusing picture at the higher energies, but the results show that the cross sections overlap in the medium energy and low energy regions. This result does not hold for tritons for which the ^{60}Ni results (and those for ^{56}Fe) are 50% higher than the ^{54}Fe. The difference can be partially explained on the basis of the indirect pickup reaction mechanism and the availability of nucleons.

In the figures, the data which has been averaged into bins of width 0.4 to 2 MeV does not show significant structure effects. At the high energies the plot is made directly from the 50 keV/channel results.

Table 3 shows the energy-integrated laboratory cross sections in units of millibarns/steradian, and the average energies in MeV, at each angle. Note that the average is performed over only the observed portion of the spectrum, that above the listed low-energy cutoffs. Tables 4-8 list for each angle the laboratory cross sections [millibarns/(steradian-MeV)] for proton-, deuteron-, triton-, helium-3-, and alpha-particle production

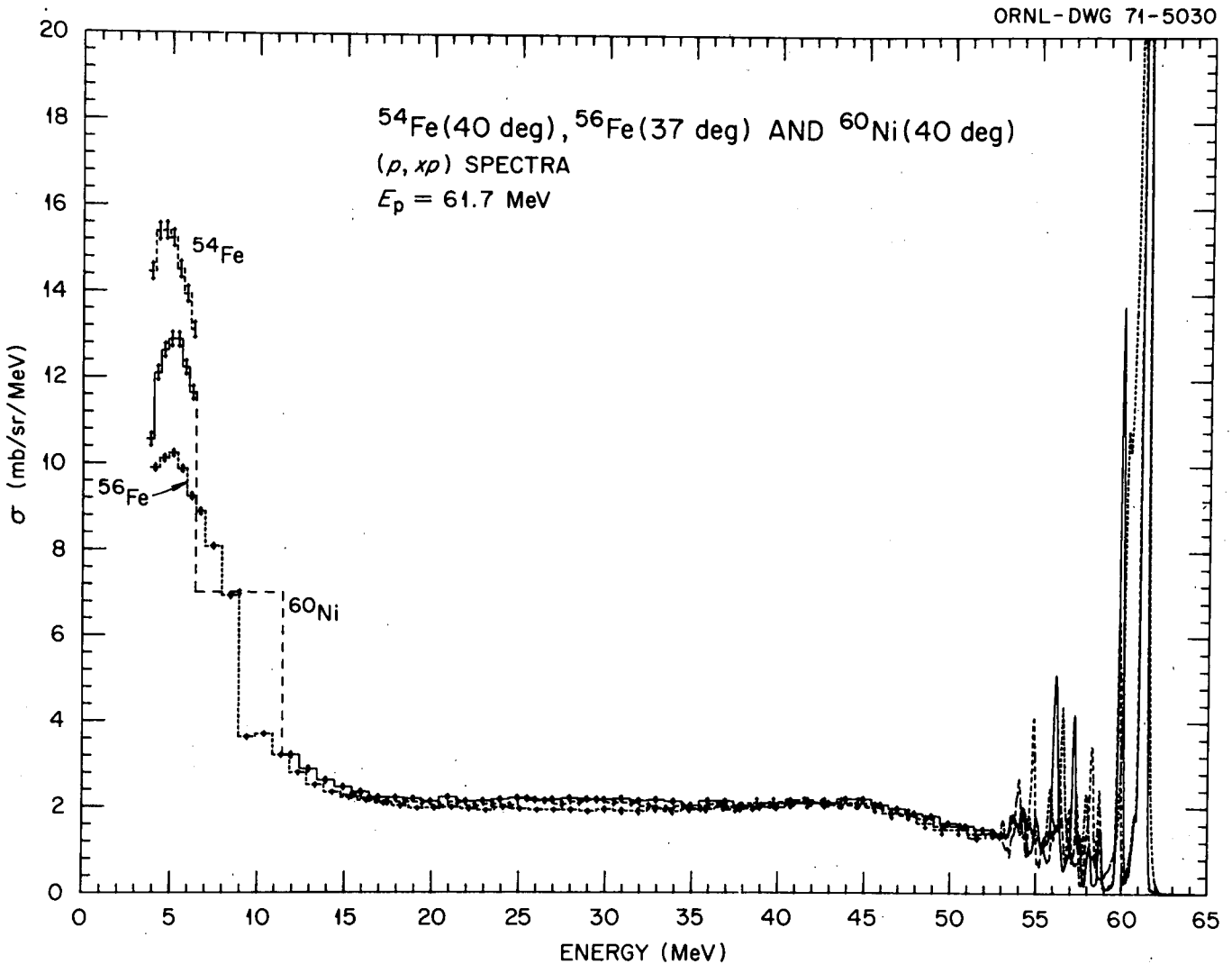

Fig. 3. Spectra from the (p,xp) Reaction for 62-MeV Protons on ^{56}Fe at 37 deg and on ^{54}Fe and ^{60}Ni at 40 deg. The broad dashed bin near 10 MeV in the otherwise-solid line represents the average cross section for ^{60}Ni(p,xp) in the region where cross sections were affected by the dead layer. A gap is shown in the ^{54}Fe(p,xp) curve from 6 to 15 MeV; beyond this energy the curves are difficult to distinguish.

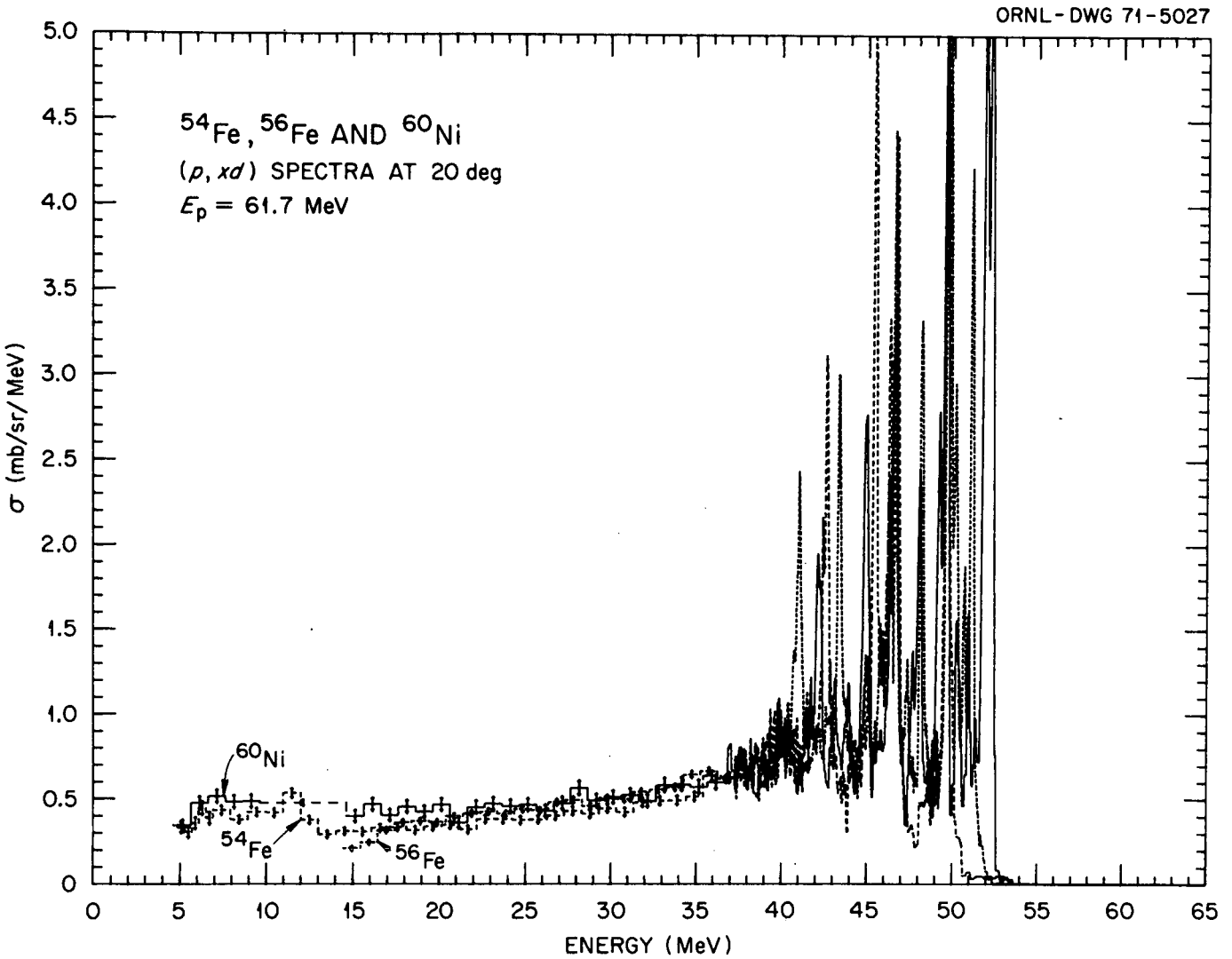

Fig. 4. Spectra from the (p,xd) Reaction for 62-MeV Protons on ^{56}Fe, ^{54}Fe, and ^{60}Ni at 20 deg. The broad dashed bin near 12 MeV in the otherwise-solid line represents the average cross section for ^{60}Ni(p,xd) in the region where cross sections were affected by the dead layer.

Table 3. Energy-Integrated Differential Cross Sections and Average Energies for 62-MeV Protons on ^{60}Ni.[a]

Lab Angle (deg)	Proton[b]			Deuteron			Triton		
	$\sigma \pm \delta\sigma$ (mb/ster)	$\bar{E}$ (MeV)	COE (MeV)	$\sigma \pm \delta\sigma$ (mb/ster)	$\bar{E}$ (MeV)	COE (MeV)	$\sigma \pm \delta\sigma$ (mb/ster)	$\bar{E}$ (MeV)	COE (MeV)
15	479 ± 2	27.6	3.6	41.2 ± 0.4	36.5	4.6	4.38 ± 0.14	27.0	5.7
20	292 ± 1	28.1	3.6	34.7 ± 0.3	35.3	4.6	3.90 ± 0.10	27.1	5.7
25	250 ± 1	26.9	3.6	25.6 ± 0.2	32.1	4.6	3.40 ± 0.07	25.0	5.7
40	170 ± 0.4	23.1	3.6	15.5 ± 0.1	27.5	4.6	2.08 ± 0.04	22.1	5.7

Lab Angle (deg)	Helium-3			Alpha		
	$\sigma \pm \delta\sigma$ (mb/ster)	$\bar{E}$ (MeV)	COE (MeV)	$\sigma \pm \delta\sigma$ (mb/ster)	$\bar{E}$ (MeV)	COE (MeV)
15	3.07 ± 0.12	33	12.5	10.4 ± 0.2	26.1	13.8
20	2.63 ± 0.08	32	12.5	9.97 ± 0.16	25.4	13.8
25	2.22 ± 0.05	31	12.5	9.29 ± 0.11	24.6	13.8
40	1.29 ± 0.03	28	12.5	6.72 ± 0.07	23.0	13.9

[a]These integrals cover the entire spectrum above the experimental cutoff energy (COE). The uncertainties shown were derived from counting uncertainties and are generally unimportant compared to the overall systematic uncertainty.

[b]Elastic proton scattering has been excluded.

from 62-MeV incident protons on ^{60}Ni, generally averaged over bins from 0.4 to 2 MeV in width. The listed bin energies are at the centers of the indicated bins. A very broad bin is shown in each table for the region affected by the extra "dead layer." Elastic proton scattering is excluded from Table 4.

ACKNOWLEDGMENTS

The authors wish to acknowledge the essential contributions of T. A. Love, N. W. Hill, and W. R. Burrus, who shared the development of the data-acquisition and analysis systems as well as the long hours of experimental runs. We also acknowledge the help of E. Beckham in setting up equipment, C. O. McNew for assistance with development and maintenance of electronic equipment and with data acquisition, P. M. Aebersold and D. I. Putzulu for imaginative work on the data analysis programs, and J. D. Drischler for help in revision of the analysis programs and in analysis and compilation of the data. We thank the ORIC operation crews for their cooperation.

REFERENCES

1. F. E. Bertrand et al., Differential Cross Sections for the Charged Particles Produced by 60-MeV Protons on Carbon, Iron, and Bismuth, ORNL-4274 (1968).

2. F. E. Bertrand and R. W. Peelle, Tabulated Cross Sections for Hydrogen and Helium Particles Produced by 62-MeV Protons on ^{89}Y, ORNL-4450 (1969); and F. E. Bertrand and R. W. Peelle, Tabulated Cross Sections for Hydrogen and Helium Particles Produced by 62- and 29-MeV Protons on ^{120}Sn, ORNL-4471 (1970).

3. N. W. Hill and W. P. Albritton, Nucl. Instr. Methods 75, 18 (1969).

4. F. E. Bertrand and R. W. Peelle, Tabulated Cross Sections for Hydrogen and Helium Particles Produced by 61-MeV Protons on ^{56}Fe, ORNL-4456 (1969); and F. E. Bertrand and R. W. Peelle, Tabulated Cross Sections for Hydrogen and Helium Particles Produced by 62-, 39-, and 29-MeV Protons on ^{54}Fe, ORNL-4469 (1970).

5. F. E. Bertrand and R. W. Peelle, Cross Sections for Hydrogen and Helium Particles Produced by 62- and 39-MeV Protons on ^{209}Bi, ORNL-4638 (1971).

6. F. E. Bertrand, et al., "A Total Absorption Detector for 60-MeV Protons Using Lithium Drifted Germanium," IEEE Trans. Nucl. Sci., NS-13, 279 (1966).

7. F. E. Bertrand, J. K. Dickens, and T. A. Love, Phys. Letters 24B, 653 (1967).

Table 4

PROTCN FROM A = 60 BOMBARDED BY 62 MEV. PROTONS.

15 DEG - RUN 5003			20 DEG - RUN 5004			25 DEG - RUN 5005			40 DEG - RUN 5006					
ENERGY (MEV)	SIGMA (MB/SR-MEV)	ERROR	ENERGY (MEV)	SIGMA (MB/SR-MEV)	ERROR	ENERGY (MEV)	SIGMA (MB/SR-MEV)	ERROR	ENERGY (MEV)	SIGMA (MB/SR-MEV)	ERROR	ENERGY (MEV)	SIGMA (MB/SR-MEV)	ERROR
3.78	14.34	0.41	3.78	11.81	0.27	3.78	12.19	0.20	3.82	10.55	0.14			
4.18	15.22	0.42	4.18	13.46	0.29	4.18	13.33	0.21	4.22	12.09	0.15			
4.58	17.38	0.45	4.58	14.51	0.30	4.58	14.02	0.21	4.62	12.63	0.16			
4.98	17.26	0.45	4.98	14.20	0.30	4.98	14.90	0.22	5.02	12.89	0.16			
5.38	17.60	0.46	5.38	15.08	0.31	5.38	14.41	0.22	5.42	12.88	0.16			
5.78	17.92	0.46	5.78	14.70	0.30	5.78	14.36	0.22	5.82	12.22	0.16			
6.18	17.49	0.45	6.18	13.88	0.30	6.18	14.03	0.21	6.22	11.64	0.15			
8.88	14.87	0.12	8.89	9.94	0.07	8.88	8.98	0.05	8.92	7.01	0.03			
11.89	10.59	0.22	11.89	5.91	0.12	11.89	4.80	0.08	11.92	3.21	0.05			
12.89	10.24	0.22	12.89	5.33	0.12	12.89	4.49	0.08	12.92	2.89	0.05			
13.89	9.67	0.21	13.89	4.83	0.11	13.89	4.07	0.07	13.92	2.62	0.05			
14.89	9.61	0.21	14.89	4.48	0.11	14.89	3.67	0.07	14.92	2.46	0.04			
15.89	9.10	0.21	15.90	4.42	0.11	15.89	3.51	0.07	15.92	2.35	0.04			
16.89	8.74	0.20	16.90	4.03	0.10	16.89	3.33	0.07	16.92	2.22	0.04			
17.89	8.62	0.20	17.90	4.00	0.10	17.89	3.13	0.06	17.92	2.22	0.04			
18.89	8.36	0.20	18.90	3.80	0.10	18.89	3.04	0.06	18.92	2.19	0.04			
19.89	8.43	0.20	19.90	3.79	0.10	19.89	2.90	0.06	19.92	2.13	0.04			
20.89	8.02	0.19	20.90	3.60	0.10	20.89	2.97	0.06	20.92	2.23	0.04			
21.89	8.09	0.20	21.90	3.40	0.09	21.90	2.81	0.06	21.92	2.13	0.04			
22.90	7.97	0.19	22.90	3.62	0.10	22.90	2.84	0.06	22.92	2.14	0.04			
23.90	7.54	0.19	23.91	3.53	0.09	23.90	2.86	0.06	23.92	2.18	0.04			
24.90	7.65	0.19	24.91	3.54	0.09	24.90	2.74	0.06	24.92	2.21	0.04			
25.90	7.37	0.19	25.91	3.49	0.09	25.90	2.83	0.06	25.92	2.17	0.04			
26.90	6.98	0.18	26.91	3.25	0.09	26.90	2.67	0.06	26.92	2.18	0.04			
27.90	6.95	0.18	27.91	3.44	0.09	27.90	2.89	0.06	27.92	2.21	0.04			
28.90	6.51	0.18	28.91	3.40	0.09	28.90	2.90	0.06	28.92	2.19	0.04			
29.90	6.53	0.18	29.91	3.36	0.09	29.90	2.98	0.06	29.92	2.17	0.04			
30.90	6.59	0.18	30.91	3.43	0.09	30.90	2.87	0.06	30.92	2.20	0.04			
31.90	6.41	0.17	31.92	3.40	0.09	31.90	2.78	0.06	31.92	2.15	0.04			
32.90	6.47	0.17	32.92	3.28	0.09	32.91	2.84	0.06	32.92	2.17	0.04			
33.91	6.14	0.17	33.92	3.40	0.09	33.91	2.84	0.06	33.92	2.14	0.04			
34.91	6.24	0.17	34.92	3.32	0.09	34.91	3.02	0.06	34.92	2.04	0.04			
35.91	6.26	0.17	35.92	3.39	0.09	35.91	2.92	0.06	35.92	2.15	0.04			
36.91	6.77	0.18	36.92	3.45	0.09	36.91	2.93	0.06	36.92	2.14	0.04			
37.91	6.93	0.18	37.92	3.62	0.10	37.91	3.00	0.06	37.92	2.04	0.04			
38.91	6.21	0.17	38.92	3.31	0.09	38.91	2.92	0.06	38.92	2.01	0.04			
39.91	6.94	0.18	39.93	3.60	0.10	39.91	3.06	0.06	39.92	2.00	0.04			
40.91	6.99	0.18	40.93	3.93	0.10	40.91	3.13	0.06	40.92	2.10	0.04			
41.91	6.99	0.18	41.93	4.08	0.10	41.91	3.20	0.06	41.92	2.10	0.04			
42.91	7.13	0.18	42.93	4.42	0.11	42.92	3.50	0.07	42.92	2.09	0.04			
43.91	7.80	0.19	43.93	4.38	0.11	43.92	3.55	0.07	43.92	2.20	0.04			
44.92	7.76	0.19	44.93	4.79	0.11	44.92	3.88	0.07	44.92	2.19	0.04			
45.92	7.80	0.19	45.93	4.68	0.11	45.92	3.70	0.07	45.92	2.06	0.04			
46.92	7.39	0.19	46.93	4.43	0.11	46.92	3.38	0.07	46.92	1.97	0.04			
47.92	6.51	0.18	47.94	3.84	0.10	47.92	3.19	0.06	47.92	1.86	0.04			
48.92	6.76	0.18	48.94	3.84	0.10	48.92	3.13	0.06	48.92	1.80	0.04			
49.92	6.33	0.17	49.94	3.50	0.09	49.92	2.87	0.06	49.92	1.64	0.04			
50.92	5.24	0.16	50.94	3.27	0.09	50.92	2.93	0.06	50.92	1.57	0.04			
51.92	5.41	0.16	51.94	3.45	0.09	51.92	2.75	0.06	51.92	1.49	0.03			
52.92	5.75	0.16	52.94	3.38	0.09	52.92	2.78	0.06	52.92	1.33	0.03			
53.92	5.34	0.16	53.94	3.44	0.09	53.93	3.08	0.06	53.92	1.74	0.04			
54.92	4.96	0.15	54.95	3.65	0.10	54.93	3.40	0.07	54.92	1.26	0.03			
55.93	4.62	0.15	55.95	3.69	0.10	55.93	3.46	0.07	55.92	2.43	0.04			
56.93	3.58	0.13	56.95	3.37	0.09	56.93	3.64	0.07	56.92	1.58	0.04			
57.93	7.997	0.195	57.95	9.033	0.151	57.93	8.839	0.107	57.92	0.698	0.023			
58.93	1.484	0.084	58.95	1.640	0.064	58.93	1.730	0.047	58.92	0.465	0.019			
59.93	7.02	0.18	59.95	11.82	0.17	59.93	7.65	0.10	59.82	4.51	0.07			
60.63	31.364	0.609	60.60	15.774	0.365	60.51	7.706	0.258	0.0	0.0	0.0			

Table 5

DEUTERON FROM A = 60 BOMBARDED BY 62 MEV. PROTONS.

15 DEG - RUN 5003			20 DEG - RUN 5004			25 DEG - RUN 5005			40 DEG - RUN 5006					
ENERGY (MEV)	SIGMA (MB/SR-MEV)	ERROR	ENERGY (MEV)	SIGMA (MB/SR-MEV)	ERROR	ENERGY (MEV)	SIGMA (MB/SR-MEV)	ERROR	ENERGY (MEV)	SIGMA (MB/SR-MEV)	ERROR	ENERGY (MEV)	SIGMA (MB/SR-MEV)	ERROR
5.13	0.345	0.040	5.13	0.343	0.029	5.13	0.357	0.021	5.12	0.357	0.017			
6.13	0.441	0.046	6.13	0.477	0.035	6.13	0.487	0.025	6.12	0.427	0.018			
7.13	0.505	0.049	7.13	0.516	0.036	7.13	0.497	0.025	7.12	0.443	0.019			
8.13	0.537	0.050	8.14	0.484	0.035	8.13	0.498	0.025	8.12	0.465	0.019			
9.13	0.509	0.049	9.14	0.487	0.035	9.13	0.513	0.026	9.12	0.445	0.019			
12.14	0.493	0.021	12.14	0.477	0.016	12.14	0.441	0.011	12.12	0.377	0.008			
15.14	0.414	0.044	15.14	0.398	0.032	15.14	0.426	0.023	15.12	0.325	0.016			
16.14	0.487	0.048	16.15	0.468	0.034	16.14	0.409	0.023	16.12	0.339	0.016			
17.14	0.414	0.044	17.15	0.404	0.032	17.14	0.429	0.024	17.12	0.297	0.015			
18.14	0.380	0.042	18.15	0.455	0.034	18.14	0.364	0.022	18.12	0.296	0.015			
19.14	0.507	0.049	19.15	0.425	0.033	19.14	0.419	0.023	19.12	0.322	0.016			
20.14	0.396	0.043	20.15	0.468	0.034	20.14	0.419	0.023	20.12	0.310	0.016			
21.14	0.407	0.044	21.15	0.360	0.030	21.14	0.412	0.023	21.12	0.304	0.016			
22.15	0.480	0.048	22.15	0.453	0.034	22.15	0.432	0.024	22.12	0.296	0.015			
23.15	0.456	0.046	23.15	0.472	0.035	23.15	0.425	0.023	23.12	0.312	0.016			
24.15	0.548	0.051	24.16	0.458	0.034	24.15	0.433	0.024	24.12	0.320	0.016			
25.15	0.516	0.049	25.16	0.466	0.034	25.15	0.432	0.024	25.12	0.317	0.016			
26.15	0.604	0.053	26.16	0.429	0.033	26.15	0.480	0.025	26.12	0.303	0.015			
27.15	0.546	0.051	27.16	0.474	0.035	27.15	0.458	0.024	27.12	0.297	0.015			
28.15	0.536	0.050	28.16	0.566	0.038	28.15	0.440	0.024	28.12	0.286	0.015			
29.15	0.705	0.058	29.16	0.492	0.035	29.15	0.470	0.025	29.12	0.285	0.015			
30.15	0.656	0.056	30.16	0.511	0.036	30.15	0.413	0.023	30.12	0.273	0.015			
31.15	0.588	0.053	31.16	0.524	0.036	31.15	0.447	0.024	31.12	0.278	0.015			
32.15	0.570	0.052	32.17	0.489	0.035	32.16	0.420	0.023	32.12	0.281	0.015			
33.16	0.660	0.056	33.17	0.583	0.038	33.16	0.416	0.023	33.12	0.249	0.014			
34.16	0.698	0.057	34.17	0.588	0.039	34.16	0.441	0.024	34.12	0.261	0.014			
35.16	0.661	0.056	35.17	0.572	0.038	35.16	0.422	0.023	35.12	0.248	0.014			
36.16	0.776	0.061	36.17	0.598	0.039	36.16	0.427	0.024	36.12	0.274	0.015			
37.16	0.800	0.062	37.17	0.700	0.042	37.16	0.422	0.023	37.12	0.278	0.015			
38.16	0.886	0.065	38.17	0.617	0.040	38.16	0.422	0.023	38.12	0.242	0.014			
39.16	0.766	0.060	39.18	0.629	0.040	39.16	0.468	0.025	39.12	0.273	0.015			
40.16	0.958	0.067	40.18	0.840	0.046	40.16	0.508	0.026	40.12	0.257	0.014			
41.16	0.950	0.067	41.18	0.689	0.042	41.16	0.510	0.026	41.12	0.308	0.016			
42.16	1.549	0.086	42.18	1.235	0.056	42.16	0.683	0.030	42.12	0.323	0.016			
43.16	1.157	0.074	43.18	0.827	0.046	43.17	0.610	0.028	43.12	0.288	0.015			
44.17	1.200	0.075	44.18	0.837	0.046	44.17	0.550	0.027	44.12	0.423	0.018			
45.17	1.702	0.090	45.18	1.390	0.059	45.17	0.892	0.034	45.12	0.231	0.013			
46.17	1.589	0.087	46.18	1.587	0.063	46.17	0.827	0.033	46.12	0.399	0.018			
47.17	1.315	0.079	47.19	1.049	0.052	47.17	0.560	0.027	47.12	0.342	0.016			
48.17	1.330	0.079	48.19	1.225	0.056	48.17	0.708	0.030	48.12	0.223	0.013			
49.17	1.810	0.093	49.19	2.118	0.073	49.17	1.403	0.043	49.12	0.568	0.021			
50.17	2.200	0.102	50.19	1.271	0.057	50.17	0.577	0.027	50.12	0.199	0.013			
51.17	0.919	0.066	51.19	0.850	0.046	51.17	0.534	0.026	51.12	0.432	0.018			
52.17	5.165	0.156	52.19	3.434	0.093	52.17	1.926	0.050	51.94	0.366	0.021			
52.97	0.022	0.013	53.09	0.026	0.009	52.90	0.015	0.007	0.0	0.0	0.0			

Table 6

TRITON FROM A = 60 BOMBARDED BY 62 MEV. PROTONS.

15 DEG - RUN 5003			20 DEG - RUN 5004			25 DEG - RUN 5005			40 DEG - RUN 5006					
ENERGY (MEV)	SIGMA (MB/SR-MEV)	ERROR	ENERGY (MEV)	SIGMA (MB/SR-MEV)	ERROR	ENERGY (MEV)	SIGMA (MB/SR-MEV)	ERROR	ENERGY (MEV)	SIGMA (MB/SR-MEV)	ERROR	ENERGY (MEV)	SIGMA (MB/SR-MEV)	ERROR
6.68	0.103	0.016	6.68	0.089	0.011	6.68	0.087	0.008	6.67	0.076	0.005			
8.68	0.105	0.016	8.69	0.086	0.010	8.68	0.097	0.008	8.67	0.083	0.006			
10.68	0.110	0.016	10.69	0.088	0.011	10.69	0.100	0.008	10.67	0.075	0.005			
14.69	0.104	0.009	14.69	0.093	0.006	14.69	0.090	0.005	14.67	0.063	0.002			
18.69	0.107	0.016	18.70	0.099	0.011	18.69	0.092	0.008	18.67	0.067	0.005			
20.69	0.100	0.015	20.70	0.084	0.010	20.69	0.091	0.008	20.67	0.063	0.005			
22.70	0.075	0.013	22.70	0.098	0.011	22.70	0.084	0.007	22.67	0.057	0.005			
24.70	0.096	0.015	24.71	0.097	0.011	24.70	0.079	0.007	24.67	0.054	0.005			
26.70	0.097	0.015	26.71	0.081	0.010	26.70	0.093	0.008	26.67	0.050	0.004			
28.70	0.081	0.014	28.71	0.092	0.011	28.70	0.088	0.008	28.67	0.043	0.004			
30.70	0.098	0.015	30.71	0.101	0.011	30.70	0.074	0.007	30.67	0.043	0.004			
32.70	0.095	0.015	32.72	0.068	0.009	32.71	0.079	0.007	32.67	0.043	0.004			
34.71	0.134	0.018	34.72	0.091	0.011	34.71	0.082	0.007	34.67	0.042	0.004			
36.71	0.148	0.019	36.72	0.120	0.012	36.71	0.074	0.007	36.67	0.040	0.004			
38.71	0.109	0.016	38.72	0.094	0.011	38.71	0.074	0.007	38.67	0.039	0.004			
40.71	0.134	0.018	40.73	0.097	0.011	40.71	0.066	0.007	40.67	0.023	0.003			
42.71	0.111	0.016	42.73	0.075	0.010	42.72	0.047	0.005	42.67	0.022	0.003			
44.72	0.070	0.013	44.73	0.062	0.009	44.72	0.049	0.006	44.67	0.011	0.002			
46.72	0.021	0.007	46.73	0.034	0.007	46.72	0.018	0.003	46.67	0.004	0.001			
48.72	0.084	0.014	48.74	0.105	0.012	48.62	0.058	0.006	48.47	0.018	0.003			
0.0	0.0	0.0	49.81	0.017	0.017	0.0	0.0	0.0	0.0	0.0	0.0			

Table 7

HELIUM-3 FROM A = 60 BOMBARDED BY 62 MEV. PROTONS.

15 DEG - RUN 5003			20 DEG - RUN 5004			25 DEG - RUN 5005			40 DEG - RUN 5006				
ENERGY (MEV)	SIGMA (MB/SR-MEV)	ERROR	ENERGY (MEV)	SIGMA (MB/SR-MEV)	ERROR	ENERGY (MEV)	SIGMA (MB/SR-MEV)	ERROR	ENERGY (MEV)	SIGMA (MB/SR-MEV)	ERROR	ENERGY (MEV)	SIGMA ERPOR (MB/SR-MEV)
13.49	0.060	0.012	13.49	0.051	0.008	13.49	0.050	0.006	13.52	0.038	0.004		
15.49	0.038	0.009	15.49	0.057	0.008	15.49	0.056	0.006	15.52	0.045	0.004		
17.49	0.073	0.013	17.50	0.065	0.009	17.49	0.052	0.006	17.52	0.041	0.004		
19.49	0.064	0.012	19.50	0.046	0.008	19.49	0.044	0.005	19.52	0.043	0.004		
21.49	0.067	0.013	21.50	0.055	0.008	21.50	0.057	0.006	21.52	0.039	0.004		
23.50	0.050	0.011	23.51	0.052	0.008	23.50	0.055	0.006	23.52	0.036	0.004		
25.50	0.055	0.011	25.51	0.054	0.008	25.50	0.058	0.006	25.52	0.036	0.004		
31.50	0.099	0.007	31.52	0.086	0.004	31.50	0.077	0.003	31.52	0.046	0.002		
37.51	0.108	0.016	37.52	0.097	0.011	37.51	0.073	0.007	37.52	0.030	0.003		
39.51	0.068	0.013	39.53	0.067	0.009	39.51	0.049	0.006	39.52	0.023	0.003		
41.51	0.118	0.017	41.53	0.108	0.012	41.51	0.070	0.007	41.52	0.029	0.003		
43.51	0.134	0.018	43.53	0.090	0.011	43.52	0.063	0.006	43.52	0.028	0.003		
45.52	0.120	0.017	45.53	0.079	0.010	45.52	0.054	0.006	45.52	0.018	0.003		
47.52	0.064	0.012	47.54	0.056	0.008	47.52	0.041	0.005	47.52	0.007	0.002		
49.02	0.035	0.013	49.14	0.008	0.004	49.02	0.008	0.003	48.64	0.000	0.001		

Table 8

ALPHA FROM A = 60 BOMBARDED BY 62 MEV. PROTONS.

15 DEG - RUN 5003			20 DEG - RUN 5004			25 DEG - RUN 5005			40 DEG - RUN 5006					
ENERGY (MEV)	SIGMA (MB/SR-MEV)	ERROR	ENERGY (MEV)	SIGMA (MB/SR-MEV)	ERROR	ENERGY (MEV)	SIGMA (MB/SR-MEV)	ERROR	ENERGY (MEV)	SIGMA (MB/SR-MEV)	ERROR	ENERGY (MEV)	SIGMA (MB/SR-MEV)	
14.29	1.25	0.08	14.29	1.20	0.06	14.29	1.15	0.04	14.37	0.95	0.03			
15.29	0.886	0.065	15.29	0.952	0.049	15.29	0.923	0.035	15.37	0.750	0.024			
16.29	0.727	0.059	16.30	0.760	0.044	16.29	0.747	0.031	16.37	0.610	0.022			
17.29	0.595	0.053	17.30	0.660	0.041	17.29	0.639	0.029	17.37	0.477	0.019			
18.29	0.533	0.050	18.30	0.515	0.036	18.29	0.541	0.026	18.37	0.392	0.018			
19.29	0.495	0.048	19.30	0.410	0.032	19.29	0.420	0.023	19.37	0.338	0.016			
20.29	0.382	0.043	20.30	0.414	0.032	20.29	0.405	0.023	20.37	0.298	0.015			
21.29	0.333	0.040	21.30	0.400	0.032	21.29	0.339	0.021	21.37	0.255	0.014			
22.30	0.317	0.039	22.30	0.280	0.027	22.30	0.299	0.020	22.37	0.247	0.014			
23.30	0.348	0.041	23.30	0.286	0.027	23.30	0.266	0.019	23.37	0.222	0.013			
24.30	0.253	0.035	24.31	0.325	0.029	24.30	0.256	0.018	24.37	0.193	0.012			
32.30	0.173	0.007	32.32	0.154	0.005	32.31	0.146	0.004	32.37	0.100	0.002			
40.31	0.145	0.026	40.33	0.126	0.018	40.31	0.121	0.013	40.37	0.064	0.007			
41.31	0.154	0.027	41.33	0.127	0.018	41.31	0.117	0.012	41.37	0.063	0.007			
42.31	0.166	0.028	42.33	0.116	0.017	42.31	0.096	0.011	42.37	0.052	0.006			
43.31	0.129	0.025	43.33	0.104	0.016	43.32	0.088	0.011	43.37	0.047	0.006			
44.32	0.086	0.020	44.33	0.098	0.016	44.32	0.080	0.010	44.37	0.043	0.006			
45.32	0.115	0.023	45.33	0.103	0.016	45.32	0.094	0.011	45.37	0.045	0.006			
46.32	0.122	0.024	46.33	0.113	0.017	46.32	0.091	0.011	46.37	0.036	0.005			
47.32	0.087	0.020	47.34	0.095	0.015	47.32	0.060	0.009	47.37	0.028	0.005			
48.32	0.054	0.016	48.34	0.090	0.015	48.32	0.056	0.009	48.37	0.034	0.005			
49.32	0.111	0.023	49.34	0.078	0.014	49.32	0.041	0.007	49.37	0.017	0.004			
50.32	0.126	0.024	50.34	0.064	0.013	50.32	0.054	0.008	50.37	0.021	0.004			
51.32	0.090	0.021	51.34	0.054	0.012	51.32	0.052	0.008	51.37	0.011	0.003			
52.32	0.061	0.017	52.34	0.066	0.013	52.32	0.043	0.007	52.37	0.011	0.003			
53.32	0.048	0.015	53.34	0.058	0.012	53.32	0.026	0.006	53.37	0.009	0.003			
54.32	0.045	0.015	54.34	0.036	0.010	54.33	0.026	0.006	54.37	0.004	0.002			
55.33	0.020	0.010	55.35	0.019	0.007	55.33	0.010	0.004	55.37	0.003	0.002			
56.33	0.014	0.008	56.35	0.013	0.006	56.33	0.012	0.004	56.37	0.003	0.002			
57.33	0.015	0.009	57.35	0.012	0.006	57.33	0.007	0.003	57.37	0.002	0.001			
58.33	0.024	0.011	58.35	0.022	0.007	58.33	0.012	0.004	58.37	0.001	0.001			
59.33	0.024	0.011	59.35	0.022	0.007	59.33	0.012	0.004	59.37	0.001	0.001			
60.33	0.024	0.011	60.35	0.022	0.007	60.33	0.012	0.004	60.37	0.001	0.001			